

Force Generation in Single Conventional Actomyosin Complexes Under High Dynamic Load

Yasuharu Takagi^{*†}, Earl E. Homsher[‡], Yale E. Goldman^{*¶}, and Henry Shuman^{*¶}

^{*}Pennsylvania Muscle Institute, [†]Department of Bioengineering and [¶]Physiology, University of Pennsylvania, Philadelphia, PA 19104, and [‡]Department of Physiology, David Geffen School of Medicine at UCLA, Los Angeles, CA 90095

SUPPLEMENTAL INFORMATION

Trap stiffness and quadrant detector sensitivity calibration⁷

To convert the voltage signals acquired from the quadrant detectors into their force equivalents, calibrations of trap stiffness and detector sensitivity are performed for each bead-actin-bead assembly trapped.

After a bead-actin-bead assembly is trapped, the actin is briefly tensioned with a load of ~5 pN and made slack by moving the two optical traps ~100nm closer together than needed to reduce the tension to zero. This substantially reduces the correlated motion of the two beads. The voltage signals corresponding to the Brownian fluctuations of each bead are collected for 5 s at 20 kHz sampling rate. The power spectrum of the forces experienced by a particle trapped in a harmonic potential undergoing Brownian diffusion is expected to be a Lorentzian function with a roll off frequency (f_c), dependent on the trap stiffness and a peak height dependent on the drag or Stoke's coefficient. Fig. S1 shows power spectra of single beads held in each trap, and the curves used to fit them. The spectra can be fit to a Lorentzian function (1,2,3) using the equation:

$$S_V(f) = S_0 \frac{1}{\left[1 + \frac{f^2}{f_c^2}\right]} \quad (\text{S1})$$

where, S_V = power spectrum (units = V^2/Hz), and f = frequency (units = Hz). For frequencies $f \ll f_c$, the power spectrum is approximately constant, S_0 , such that:

$$S_V(f) \cong S_0 = \frac{4\gamma k_B T}{C^2} \quad (\text{S2})$$

where, k_B = Boltzmann's constant, γ = the viscous drag coefficient of the particle (units = $\text{N}\cdot\text{s}\cdot\text{m}^{-1}$), T = the absolute temperature, and C = the calibration constant to convert the voltage measurement from the photodiode into its force equivalent (units = $\text{pN}\cdot\text{V}^{-1}$). Fitting the data with the Lorentzian of Eq. S2, gives values of the calibration constant C and trap stiffness κ_{trap} for each trapped bead from estimates of S_0 , f_c ,

$$C = \sqrt{\frac{4\gamma k_B T}{S_0}} \quad (\text{S3})$$

and,

$$\kappa = 2\pi\gamma f_c \quad (\text{S4})$$

where $\gamma = 6\pi\eta r$, $\eta \cong 0.001 \text{ N}\cdot\text{s}\cdot\text{m}^{-2}$ and r = radius of the trapped polystyrene bead = $0.55 \mu\text{m}$.

SUPPLEMENTAL FIGURE LEGENDS

FIGURE S1. Power spectrum analysis to determine trap stiffness and detector sensitivity.

The power spectra of both traps with $1.1 \mu\text{m}$ diameter polystyrene beads trapped close to the surface of the experimental chamber are shown. Fits were performed as shown

previously (1,2,3) to determine the corner frequency (f_c) and photodiode sensitivity (C). Motor trap: $f_c = 1080$ Hz; $C = 12.1$ pN·V⁻¹; Transducer trap: $f_c = 1010$ Hz; $C = 9.16$ pN·V⁻¹. The corresponding stiffnesses (κ_{trap}) of each trap are 0.066 pN/nm.

FIGURE S2. Adjustment of the isometric clamp feedback gain. The response time of the isometric clamp was calibrated by trapping a pre-tensioned (~5 pN) bead-actin-bead assembly. A square wave command signal was applied as a perturbation, and the error signal on the transducer bead was measured. The $t_{1/2}$ of the recovery of the error signal was 1 ms (top graph) and 10 ms (bottom graph) for two different feedback loop gains. Only integral gain was applied for the two feedback settings.

FIGURE S3. A histogram of the co-variance of the Brownian motions of the two beads at the ends of an actin filament during transient interactions with myosin. The histogram was calculated for 60 s of data (a representative sample is shown in Figure 4 of the main text) of interactions acquired with no feedback using a window size of 1 ms. The histogram was fit with two Gaussian peaks. For this example, the higher-variance peak, corresponding to the Brownian motion of a free bead-actin-bead assembly, was centered at ~1.04 pN² with a σ of ~0.49 pN². The lower-variance peak, corresponding to the actomyosin attached state was centered at ~0.27 pN² with a σ of ~0.17 pN². These two peaks are well separated and thus, the bound and unbound states are easily distinguished.

FIGURE S4. Schematic showing the motions of actomyosin and attached beads when acting on an immovable load (A-C) and when acting on the isometric clamp (D-G). A

and D: Before attachment an actin binding site is immediately opposite a myosin head. B and E: Following myosin binding to actin there is no net displacement of actin or beads. C: After a power stroke the internal series elasticity of myosin (e.g. an elastic element in S2 or in the light chain domain) is stretched without displacing actin when it acts on an immovable load. F: If the trap stiffness is much lower than the myosin elasticity the actin-bead assembly moves to the left rapidly and the feedback loop begins to act to restore the transducer bead to its original position. G: When the transducer bead is restored to its original position the feedback stops pulling further, the position of the myosin head is restored to its original position and its series elasticity is stretched the same amount as for an immovable load in C.

FIGURE S5. Simulated (a) duration and (b) peak force distributions at two different feedback gains using rates that are independent of load. The differential equations included in the appendix were solved numerically to determine the probability distribution of events for a load independent model.

FIGURE S6. Simulated (a) duration and (b) peak force distributions at two different feedback gains using a rate that is load dependent. The differential equations included in the appendix were solved numerically to determine the probability distribution of events for a model with only k_{23} load dependent.

FIGURE S7. Simulated (a) duration and (b) peak force distributions at two different feedback gains using a rate that is load dependent. The differential equations included in

the appendix were solved numerically to determine the probability distribution of events for a model with only k_{34} load dependent.

FIGURE S8. Simulated (a) duration and (b) peak force duration distributions at two different feedback gains using a rate that is load dependent. The differential equations included in the appendix were solved numerically to determine the probability distribution of events for a model with only k_{21} load dependent.

References

1. Svoboda, K., and S. M. Block. 1994. Biological applications of optical forces. *Annu. Rev. Biophys. Biomol. Struct.* 23:247-285.
2. Gittes, F., and C. F. Schmidt. 1998. Signals and noise in micromechanical measurements. *Methods Cell Biol.* 55:129-156.
3. Veigel, C., M. L. Bartoo, D. C. White, J. C. Sparrow, and J. E. Molloy. 1998. The stiffness of rabbit skeletal actomyosin cross-bridges determined with an optical tweezers transducer. *Biophys. J.* 75:1424-1438.

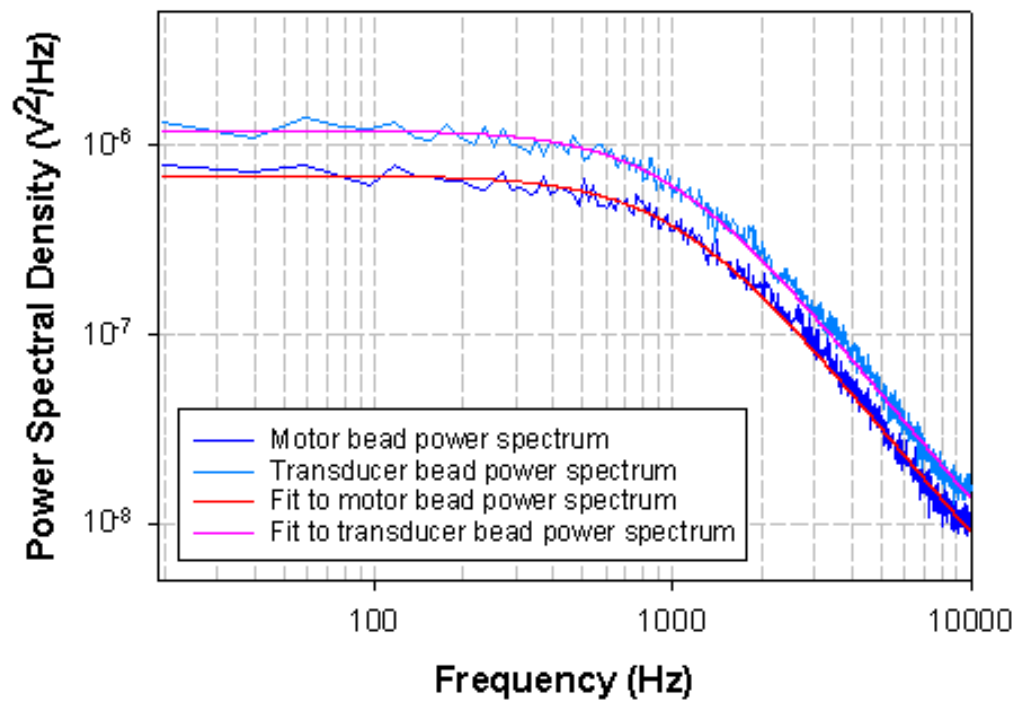


Figure S1

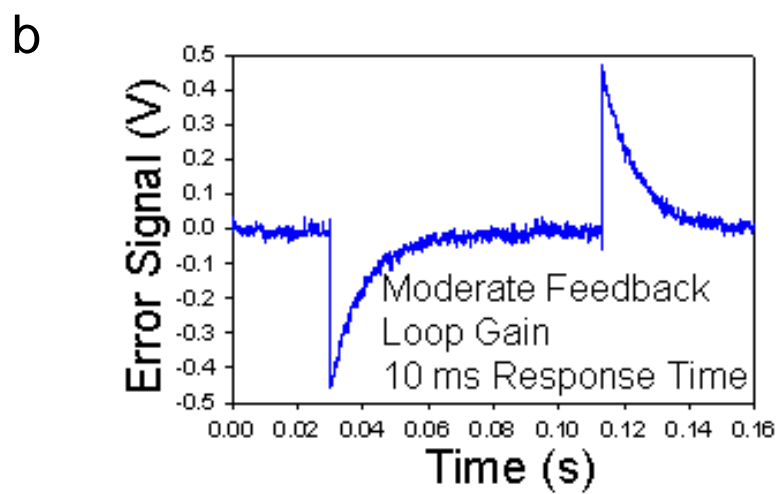
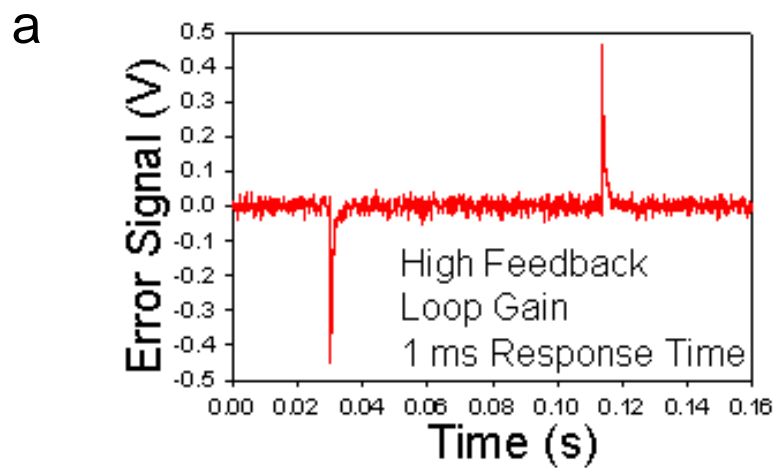


Figure S2

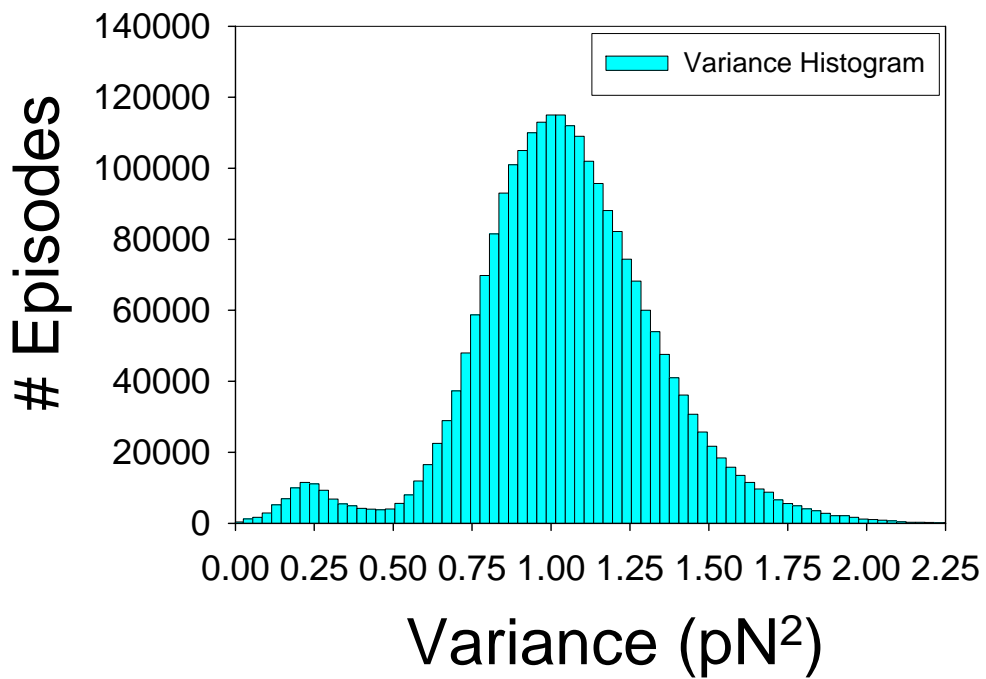


Figure S3

Immovable load

Isometric Clamp

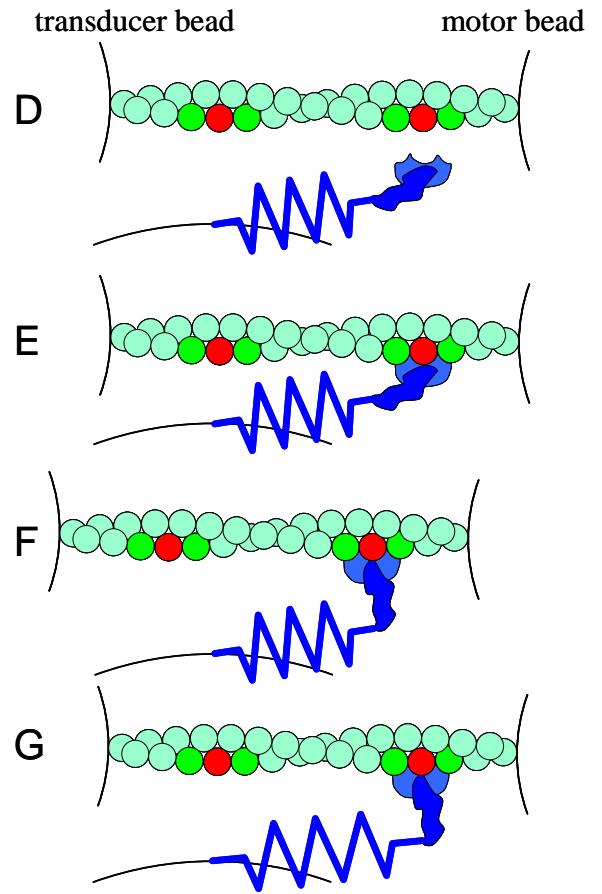
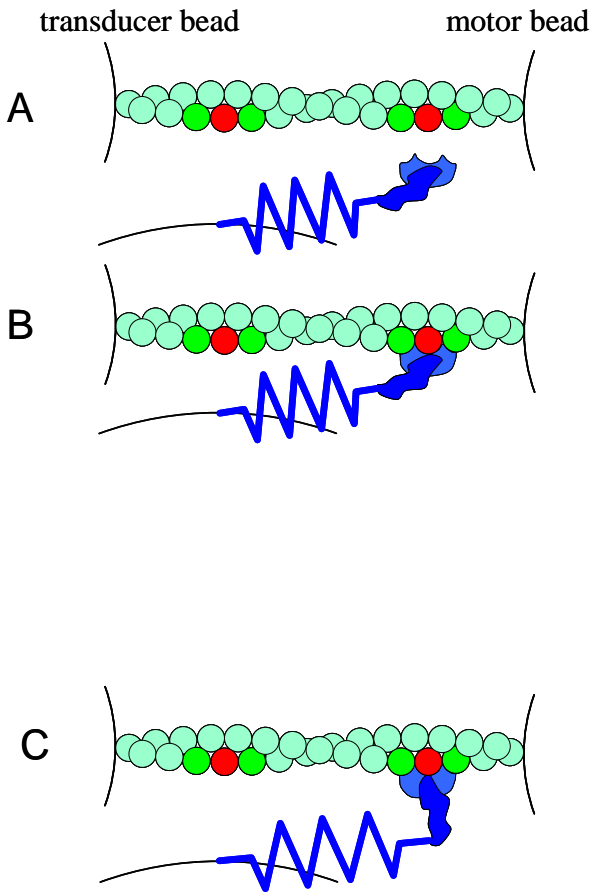


Figure S4

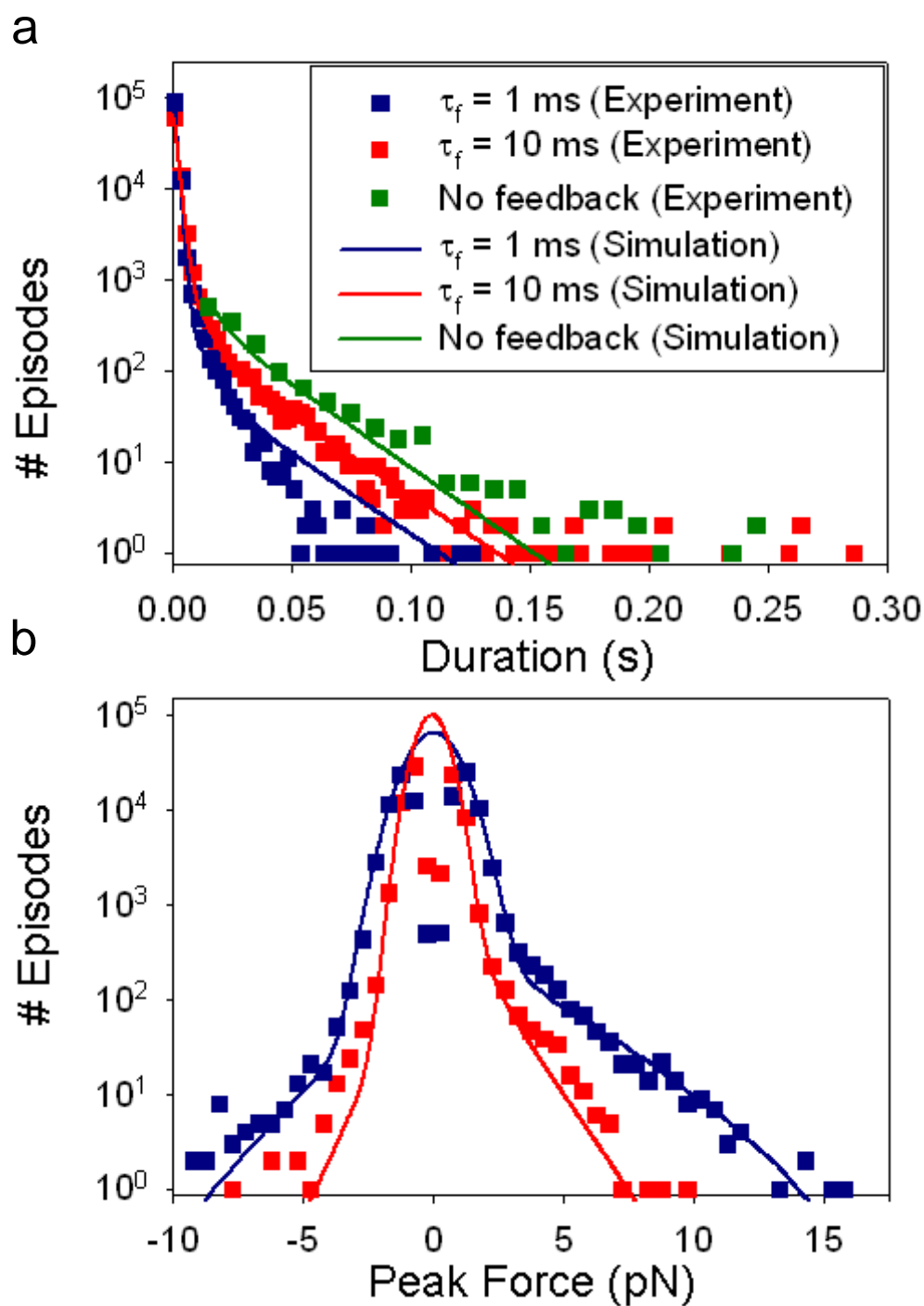


Figure S5

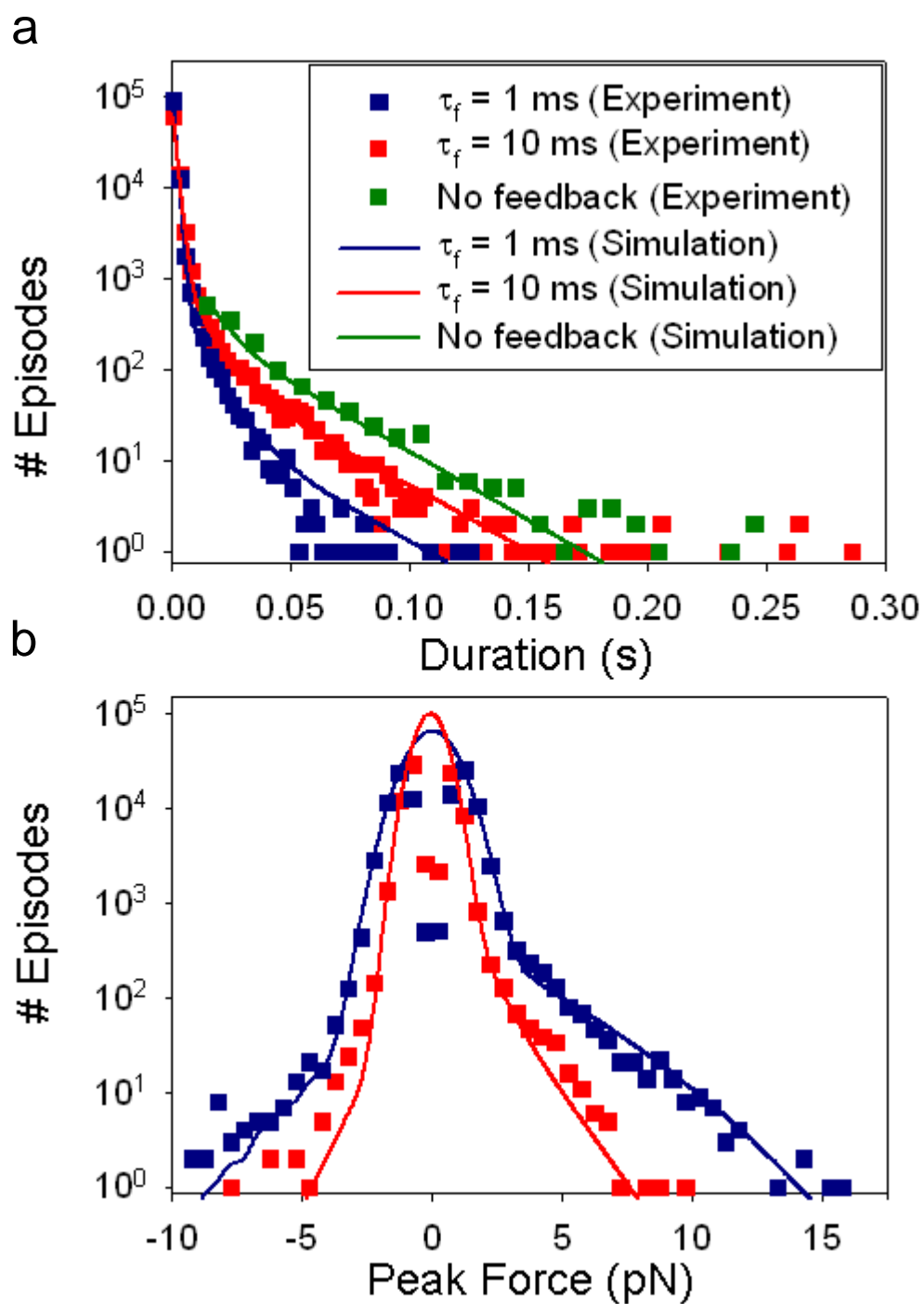


Figure S6

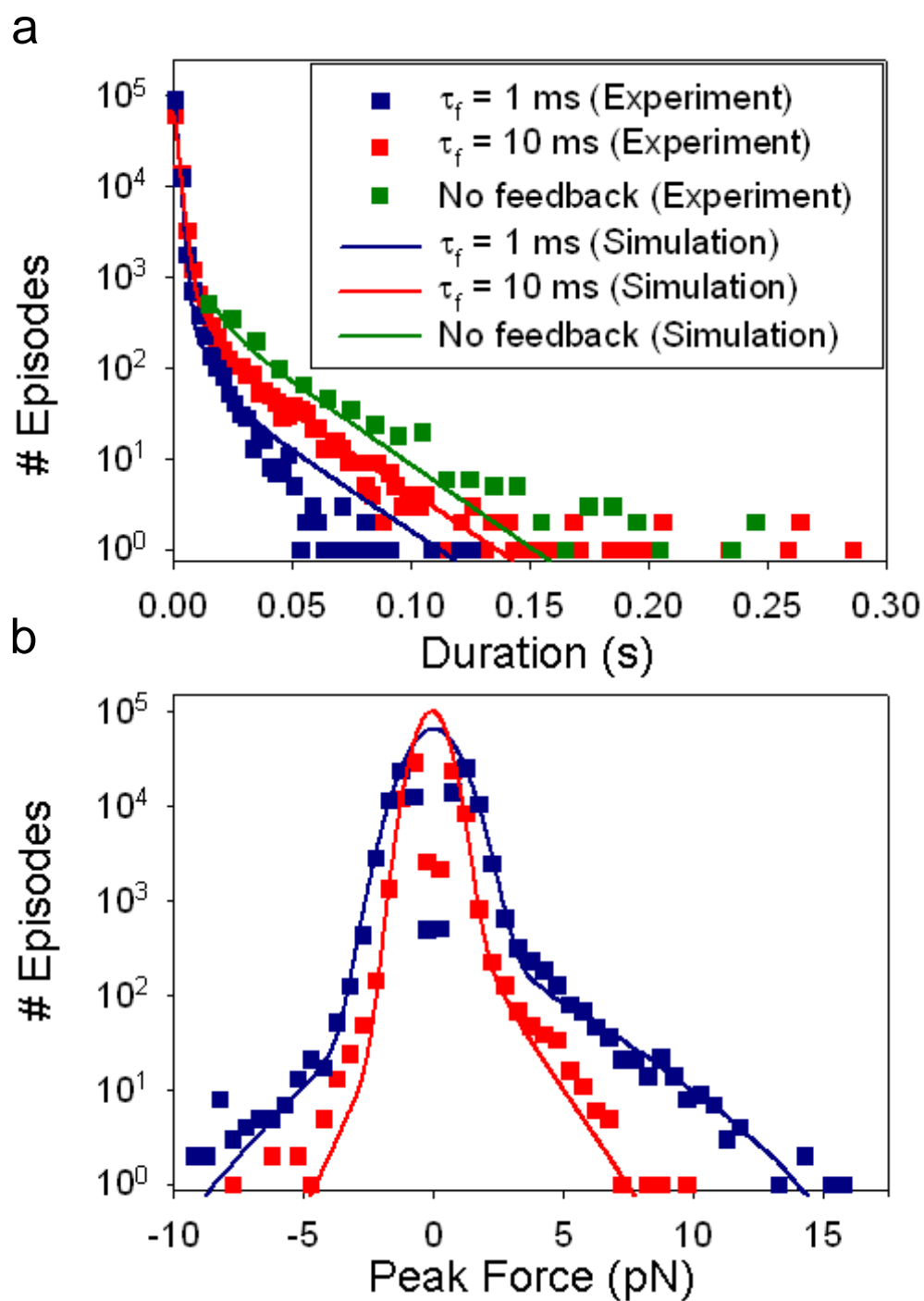


Figure S7

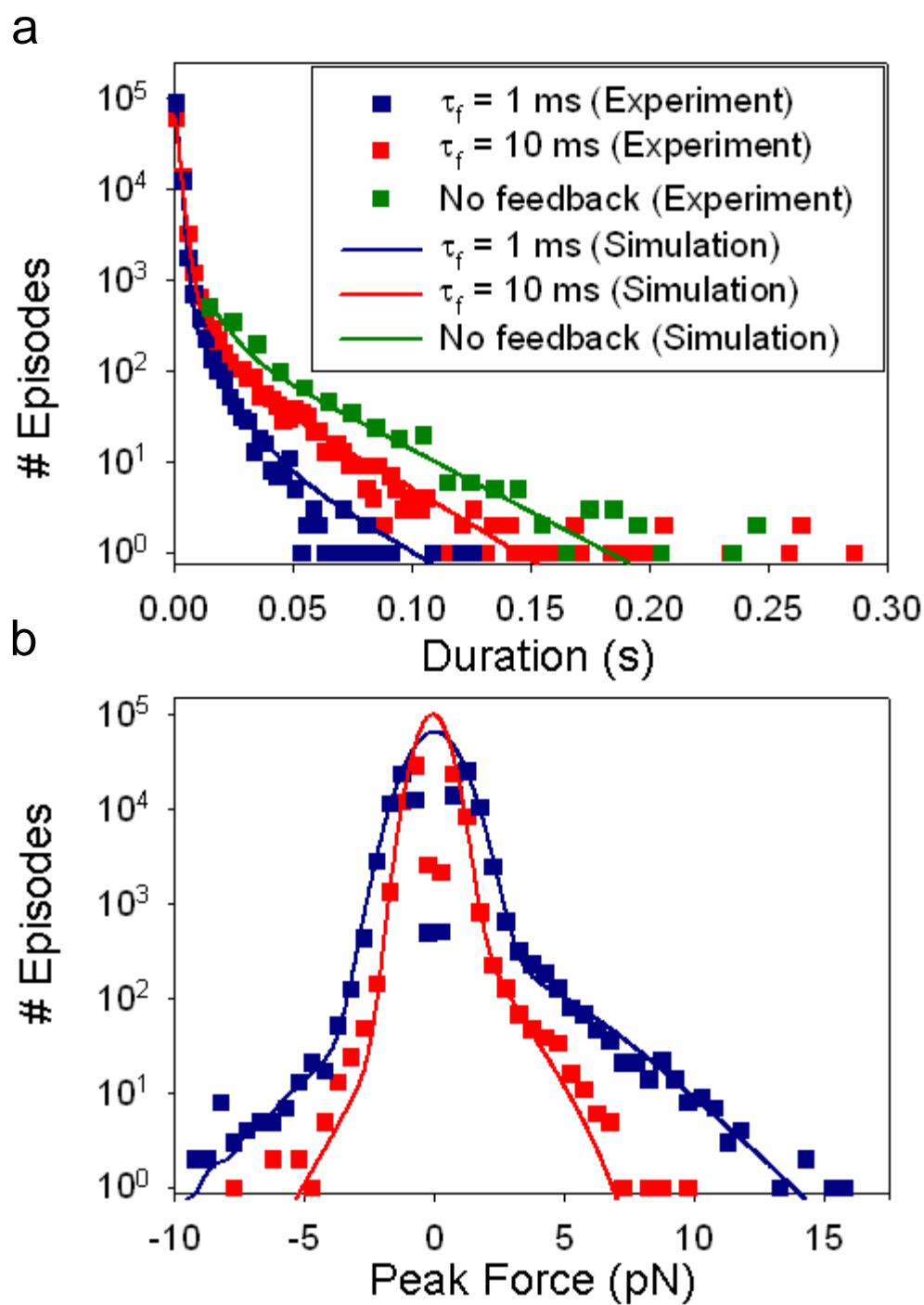


Figure S8